Hindawi Publishing Corporation
International Journal of Rotating Machinery
Volume 2015, Article ID 825835, 10 pages
http://dx.doi.org/10.1155/2015/825835

Research Article

Analysis and Simulation on UMP and EMT Characters of Turbogenerator under Axial Air-Gap Eccentricity

Yu-Ling He, Wei-Qi Deng, and Gui-Ji Tang

Department of Mechanical Engineering, North China Electric Power University, Baoding 071003, China

Correspondence should be addressed to Yu-Ling He; heyuling1@163.com

Received 26 July 2015; Revised 28 October 2015; Accepted 4 November 2015

Academic Editor: Paolo Pennacchi

The purpose of this paper is to investigate the effect of the axial air-gap eccentricity (AAGE) on the electromagnetic characters such as the axial unbalanced magnetic pull (UMP) and the electromagnetic torque (EMT). Firstly, the theoretical model of AAGE is set up, and the formulas of the axial UMP and EMT are deduced. Then the simulation study of a SDF-9 nonsalient pole synchronous generator is taken with Ansoft Maxwell to calculate the detailed axial UMPs and EMTs under normal condition and five AAGE conditions, respectively, with 2 mm to 10 mm rotor displacements. It is shown that an apparent axial UMP will be produced due to AAGE, while EMT and the phase current will be decreased. In addition, the magnetic flux density (MFD) on the stator end and the rotor end, which are more far from the center position of the stator core in the axial direction, will be decreased, while the MFD on the other ends will be generally kept stable. As AAGE develops, the axial UMP will be increased, while EMT and the phase current will be decreased. The proposed work offers a reference for the fault diagnosis and monitoring on AAGE.

1. Introduction

The air-gap between the stator and the rotor will be of asymmetry due to different causes such as the bad assembling and the serious performing condition. Then the air will be more on one side but in the meanwhile less on the other side. This is usually called air-gap eccentricity, which can be induced by the bearing offset, the deformation of the stator core, and so forth. By far, the air-gap eccentricity is primarily focused on the radial one [1–5], while actually there is also axial air-gap eccentricity (AAGE) existing. AAGE can be caused, for example, by the axial displacement of the rotor, frequently occurring in the hydrogenerators [6–8] and also happening in the turbogenerators from time to time.

There are two kinds of AAGE. The first one is static and the other one is dynamic, as indicated in Figure 1. In most cases, AAGE in turbogenerators is a static one, while the dynamic one rarely takes places except some special conditions such as oil-taking in the center hole of the rotor. This paper mainly pays attention to the static AAGE.

By far, people have paid much attention to the radial UMPs [1–5], while the studies on the axial UMP are much less. The earliest study on the axial UMP that has been found is about a calculation method based on the conducting paper model [9]. Then, another axial UMP analysis method based on the *conformal transformation* is also developed [10, 11]. However, these studies only focus on the theoretical qualitative analysis, while the quantitative analysis and the detailed UMP values are not studied. As an improvement, this paper carries out a quantitative analysis based on the simulation modeled for a SDF-9 type generator under AAGE conditions.

2. Theoretical Analysis

2.1. UMP Calculation via Conformal Transformation. Since the end electromagnetic field inside the turbogenerator is complex, usually, it is simplified by the *conformal transformation* before the further calculation. Then the complex field parameters can be calculated based on the *Schwarz-Christoffel transformation equation*.

For the sake of convenience, the stator end winding is neglected in this paper, only considering the stator end plane and the rotor end plane. Meanwhile, the effective length of

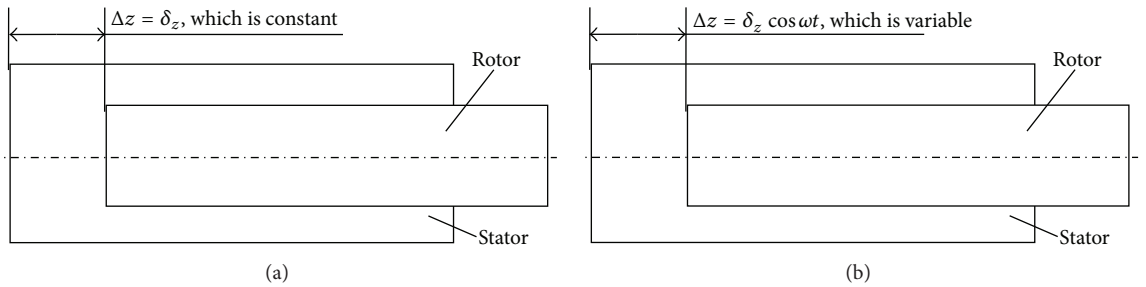

Figure 1: Two kinds of AAGE: (a) static and (b) dynamic.

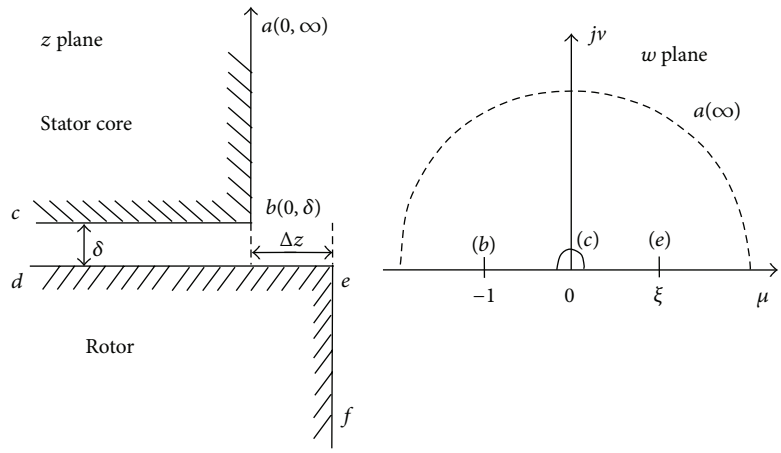

Figure 2: z-w plane mapping relation.

the stator is treated to be as long as that of the rotor. According to the *conformal transformation*, the end electromagnetic field after simplification can be indicated as Figure 2, and the points in z plane can be transformed to the vertexes in w plane, as shown in Table 1. Further, substituting the three points −1, 0, and ξ into the *Kueck transformation* equation, it has [12]

$$\frac{dz}{dw} = A_1 (w+1)^{3/2-1} (w-x)^{3/2-1} (w-0)^{0-1}; \quad (1)$$

then

$$\begin{aligned} z &= A_1 \int \frac{\sqrt{(w+1)(w-\xi)}}{w} dw + B_1 \\ &= A_1 \left[\sqrt{(w+1)(w-\xi)} \right. \\ &+ \frac{1-\xi}{2} \ln \left(\sqrt{w+1} - \sqrt{w-\xi} \right)^2 \\ &\left. - \sqrt{\xi} \arcsin \frac{(1-\xi) w - 2\xi}{w(1+\xi)} \right] + B_1, \end{aligned} \quad (2)$$

Table 1: Mapping relation between the points in w plane and the polygon vertexes in z plane.

	z	α_k	μ_k
a	∞	$-\pi$	∞
b	δ	$3\pi/2$	-1
c	∞	0	0
e	Δz	$3\pi/2$	ξ

where A_1, B_1, and ξ can be calculated by using the coordinate values of b, $c(d)$, and e, respectively, in z plane and w plane and finally written as

$$\begin{aligned} A_1 &= -\frac{j\delta}{\left(\sqrt{\xi}\pi\right)}, \\ B_1 &= \Delta z - j\frac{\delta}{\sqrt{\xi}\pi} \left[\frac{1-\delta}{2} \ln(1+\xi) + \frac{\sqrt{\xi}\pi}{2} \right], \\ \sqrt{\xi} &= \frac{\Delta z}{\delta} + \sqrt{\left(\frac{\Delta z}{\delta}\right)^2 + 1}, \end{aligned} \quad (3)$$

where δ is the radial air-gap length and Δz is the value of AAGE.

Table 2: Primary parameters of SDF-9 type generator.

Rated capacity	7.5 kVA	Axial length	$L_0 = 100$ mm
Rated voltage	400 V	Number of stator slots	$Z_1 = 24$
Power factor	0.8	Ratio of pitch to polar distance	$K_y = y/\tau = 0.83$
Rated speed	$n_r = 3000$ rpm	Pitch-shortening value	$k_p = 0.966$
Number of pole-pairs	$p = 1$	Distribution coefficient	$k_d = 0.958$
Radial air-gap length	$\delta = 0.8$ mm	Number of parallel branches	$\alpha = 2$

The permeability on the rotor end ferromagnetic boundary is thought to be infinite, and meanwhile the magnetic lines are perpendicular to the boundary. According to [11], the axial UMP on the rotor can be deduced based on (1) to (3) and indicated as

$$F = \int_0^{2\pi R} \frac{\mu_0 \psi^2}{\pi\delta} dx \cdot \left(-\arcsin \frac{1 - \left[\Delta z/\delta + \sqrt{(\Delta z/\delta)^2 + 1}\right]^2}{1 + \left[\Delta z/\delta + \sqrt{(\Delta z/\delta)^2 + 1}\right]^2} \right), \quad (4)$$

$$\psi = \int_{\text{stator}}^{\text{rotor}} H\, dl = H_{\text{rotor}} - H_{\text{stator}} = \frac{(B_{\text{rotor}} - B_{\text{stator}})}{\mu_0},$$

where δ and Δz have the same meaning as previously mentioned, R is the radius of the rotor, ψ is the magnetic difference of potential (MDP) between the rotor and the stator, H is the magnetic field intensity, B is the magnetic flux density, and μ_0 is the air permeability.

Taking the SDF-9 type nonesalient pole synchronous generator in the National Key Lab of New Energy and Electric Power System at North China Electric Power University, as an example, the detailed UMP values in the cases of 2 mm, 4 mm, and 6 mm AAGE are shown in Figure 3. The generator is of three phases and has 24 stator slots. The diameter of the rotor is 158.4 mm, and the magnetic difference of potential (MDP) between the stator end and the rotor end is proximately set to 37 A. More information about the generator can be found in Table 2 and Figure 6.

As indicated in Figure 3, it is easy to find that the AAGE will cause axial UMPs on the rotor. Moreover, the more the AAGE is, the larger the axial UMP will be. However, the mapping relation between the axial UMP and the AAGE is not linear. As the AAGE is increased to a certain extent, the axial UMP will be somewhat like saturated.

However, the precision of the calculated UMP based on (4) depends on the accuracy of the MDP, which is actually not easy to be obtained with a qualified accuracy. Besides the conformal transformation, there is another effective way to calculate the axial UMP. This method is based on the conducting paper model [9], as deduced in the following Section 2.2.

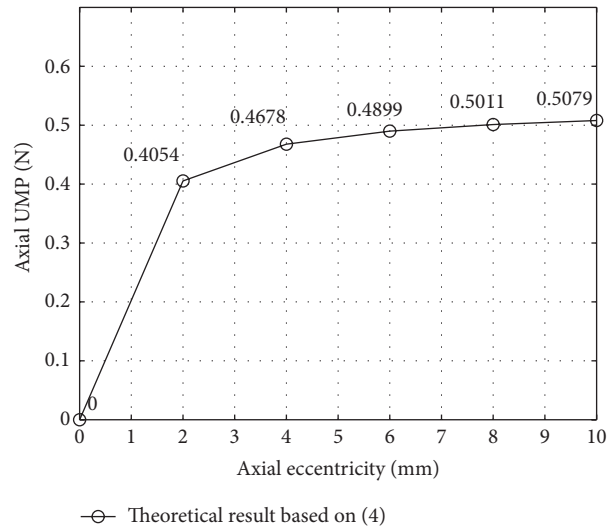

Figure 3: Relationship between AAGE and UMP based on (4).

2.2. UMP Analysis via Conducting Paper Model. The permeability on the rotor end ferromagnetic boundary is thought to be infinite, and meanwhile the magnetic lines are perpendicular to the boundary. According to [9], the axial UMP on the rotor can be deduced and indicated as

$$F = 0.0117a \left(\frac{60}{f}\right) \frac{E_0 I_{m0}}{l_0} \left(\frac{l_0}{l}\right)^2 \cdot \sum \left[\left(\frac{\partial l}{\partial x}\right)_{\text{ends}} + \left(\frac{\partial l}{\partial x}\right)_{\text{ducts}} \right], \quad (5)$$

where a is the number of phases, f is the frequency, l is the effective stator (rotor) length, l_0 is the actual stator (rotor) length (inches), E_0 and I_{m0} are the effective values of the phase voltage and the phase current at the magnetic neutral position, respectively, $\partial l/\partial x$ is the change rate of the effective machine length with respect to axial displacements, including the ends and the ducts, and F is the axial UMP (pounds).

In this paper, for the sake of convenience, the ventilating ducts are not taken into account due to their small effect. Changing the units into SI system, (5) can be transformed to

$$F = 1.32245a \left(\frac{60}{f}\right) \frac{E_0 I_{m0}}{l_0} \left(\frac{l_0}{l}\right)^2 \left(\frac{\partial l}{\partial x}\right)_{\text{ends}}. \quad (6)$$

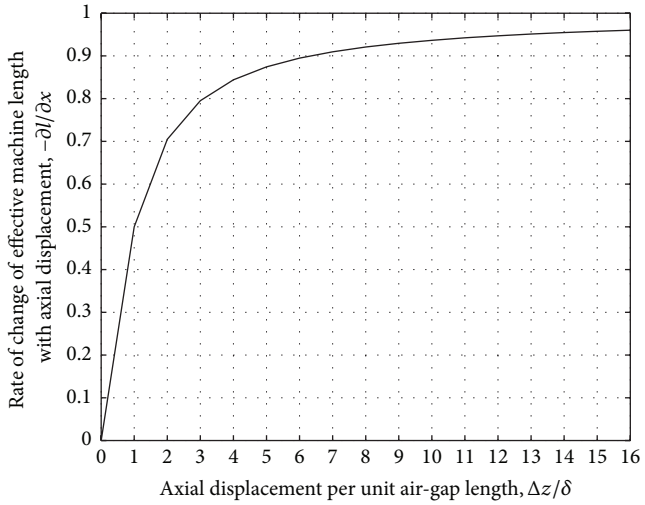

Figure 4: Change rate of effective machine length due to AAGE.

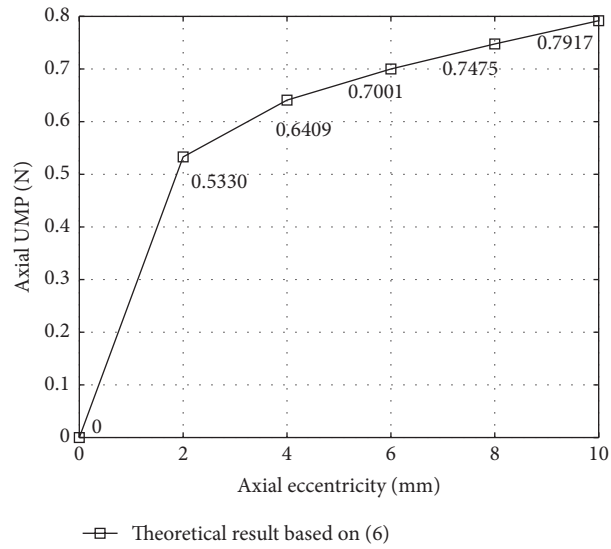

Figure 5: Relationship between AAGE and UMP based on (6).

Table 3: Relationship between $\Delta z/\delta$, $\partial l/\partial x$, and l.

AAGEs	$\Delta z/\delta$	$\partial l/\partial x$	l
0	0	0	100
2	2.5	0.7578	98
4	5	0.8743	96
6	7.5	0.9156	94
8	10	0.9365	92
10	12.5	0.9492	90

Table 4: Values of E_0 and I_{m0}.

	Voltage (V)			Current (I)		
Phase	A	B	C	A	B	C
Peak value	23.18	26.19	24.18	1.14	1.16	1.16
	23.38	26.47	24.03	1.16	1.16	1.16
Average peak value	23.28	26.33	24.11	1.15	1.16	1.16
Effective value	16.46	18.62	17.04	0.81	0.82	0.82
Average effective value	17.3733 (E_0)			0.8167 (I_{m0})		

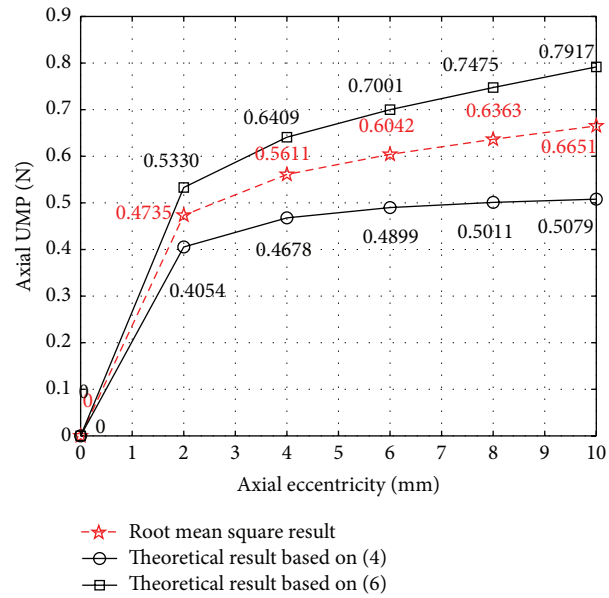

Figure 6: Relationship between AAGE and UMP based on RMS method.

The development of expressions for $\partial l/\partial x$ for the ends and the contribution of the ends to l_0/l can be calculated by (7) and finally displayed as Figure 4:

$$-\frac{\partial l}{\partial x} = \left[1 - \frac{2}{\pi}\mathrm{ctn}^{-1}\left(\frac{\Delta z}{\delta}\right)\right], \quad l = l_0 - \Delta z. \tag{7}$$

Also taking the SDF-9 type nonesalient pole synchronous generator as an example, the values of $\partial l/\partial x$ under different AAGEs are shown in Table 3.

Adding the data in Table 3 to (2), together with the data of E_0 and I_{m0} indicated in Table 4, the axial UMP results are shown in Figure 5.

As indicated in Figure 5, the same result can be found that AAGE will cause apparent axial UMPs on the rotor. Moreover, the more the AAGE is, the larger the axial UMP will be. And the mapping relation between the axial UMP and AAGE is not linear. Generally, the developing tendency of the axial UMP and the curve shape shown in Figure 5 are in accordance with those in Figure 3.

However, comparing the results in Figure 5 with that in Figure 3, it is obvious that the calculated axial force based on (6) is larger than that obtained from (4). Then the further question is to analyze the errors of these two methods. Since

the conformal transformation method (4) does not take the effect of the rotor and stator windings into account [11], qualitatively, it is easy to deduce that the axial force obtained by this method is smaller than the exactly actual value (the windings will also have an electromagnetic force which will act on the rotor and the stator as well).

In the conducting paper model method, the magnetic lines are thought to be perpendicular to the boundary [9], while actually they are not. Meanwhile, the magnetic saturation of the tooth tips is not taken into account, either [9]. Therefore, these will cause calculated axial UMP larger than the actual value. (On one hand, the axial force is in proportion to the square value of $B\cos\alpha$, B being the magnetic flux density and α being the angle between the magnetic flux lines and the boundary. On the other hand, the neglect of the saturation effect will also make the calculated value of the magnetic flux density larger than the exact one, because the practical magnetic flux density with the saturation is not linear and therefore will be smaller).

So the further problem is how to improve the accuracy of these two methods. The common operation is to take the stator and rotor windings into account for the conformal transformation method and calculate the actual magnetic flux density in detail for the conducting paper model method. However, it is not so easy to carry out these operations; for example, in the conducting paper model, the effect of the angle α between the magnetic flux lines and the boundary has to be transferred to the corresponding parameters indicated in (6). During the transforming process, it contains much work and to ensure the transfer accuracy there are still many influential factors.

In this paper, we propose a new RMS (root mean square) method combining the previous two methods together; see the next section.

2.3. UMP Analysis via a New RMS Method. The key thought of the RMS method is to neutralize the errors of the previous two methods, and the detailed calculation method is

$$F_1 = \int_0^{2\pi R} \frac{\mu_0 \psi^2}{\pi\delta} dx \cdot \left\{ -\arcsin \frac{1 - \left[\Delta z/\delta + \sqrt{[\Delta z/\delta]^2 + 1}\right]^2}{1 + \left[\Delta z/\delta + \sqrt{[\Delta z/\delta]^2 + 1}\right]^2} \right\},$$
$$F_2 = 1.32245a \left(\frac{60}{f}\right) \frac{E_0 I_{m0}}{l_0} \left(\frac{l_0}{l}\right)^2 \left(\frac{\partial l}{\partial x}\right)_{\text{ends}}, \quad (8)$$
$$F_3 = \sqrt{\frac{F_1^2 + F_2^2}{2}}.$$

The physical meaning of the proposed RMS method can be treated as the composite effective value of the conformal transformation method and the conducting paper model method. Still taking the SDF-9 type generator as an example, the axial UMP values calculated by this method and the comparison with the previous two methods are indicated in Figure 6. The accuracy of the proposed method and its improvement will be discussed in the simulation study section.

2.4. EMT Analysis. The electromagnetic torque in turbogenerators can be written as [13]

$$T_e = -\kappa_c \frac{\pi}{2} p^2 F_s \Phi \sin\left(p\delta_1\right),$$
$$\Phi = \frac{2}{\pi} Bl\tau, \quad (9)$$

where T_e is EMT, κ_c is the correction factor, p is the number of the pole-pairs, F_s is the magnetomotive force (MMF) of the stator, Φ is the magnetic flux, $p\delta_1$ is the electrical angle between the stator MMF and the composite air-gap MMF, B is the magnetic flux density, and l is the effective axial length of the air-gap.

As AAGE takes place, the effective air-gap length l in the axial direction will be decreased. Therefore, obviously, the electromagnetic torque will be decreased.

3. Simulation Study

3.1. Simulating Method and Set. The simulating model is set up for the SDF-9 type nonesalient pole synchronous generator which has been mentioned previously in the theoretical analysis section. It is a fault simulating generator which is able to carry out the stator and rotor interturn short circuit faults and the radial air-gap eccentricity fault, as indicated in Figure 7(a). However, it is not able to simulate AAGE fault and therefore here it has to take a simulation work instead. The primary parameters of the generator are shown in Table 2, according to which the 3D model for the simulation in the software Ansoft 15.0 is set up, as indicated in Figure 7(b).

The simulation is taken in a transient condition. The exciting winding and the stator winding are coupled with the special external circuits to perform the excitation, as indicated in Figures 7(c) and 7(d). During the simulation, the time step is 0.0002 s and the stop time is 0.04 s. The rotor object is selected to assign the force and the electromagnetic torque parameters. The exciting current is set to 0.4 A by using a DC source in the external circuit and the rotating speed of the rotation band is set to 3000 r/min (50 Hz). The whole simulating work follows the following steps.

(1) The generator performs normally, with no AAGE, and the axial UMP and EMT are collected as the reference samplings. The phase voltage and the phase current in normal condition are shown in Figures 8 and 9.

(2) The rotor is shifted along the axial direction (z direction; see Figure 7(b)) by 2 mm, 4 mm, 6 mm, 8 mm, and 10 mm each time, respectively, to simulate different fault degrees of AAGE and then the axial UMPs and EMTs are sampled as well to make a comparison with the normal ones.

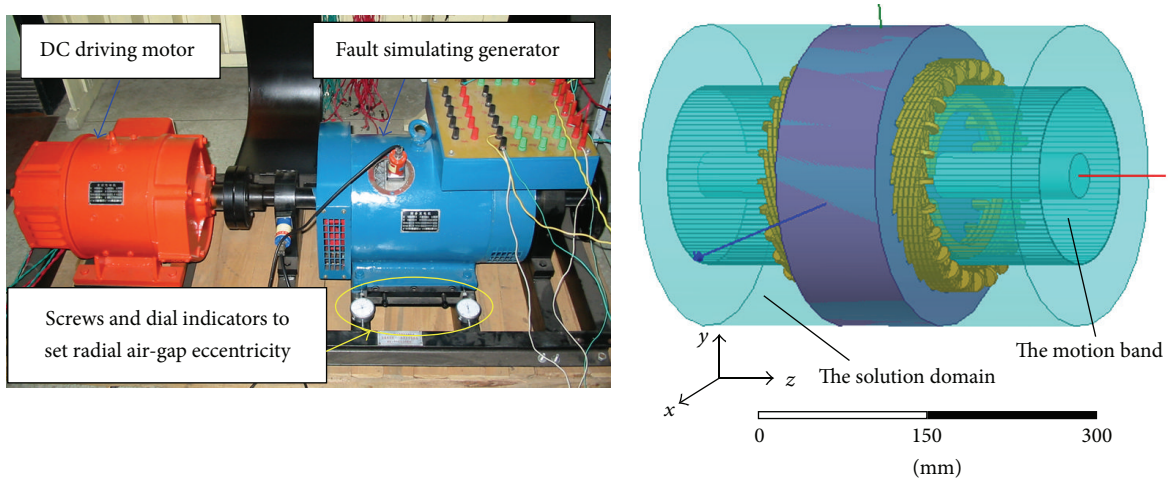

(a) Physical model of SDF-9 type generator

(b) Simulation model of SDF-9 type generator

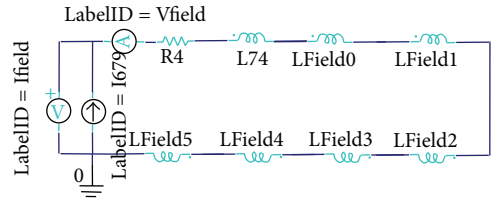

(c) External coupling circuit for the field winding

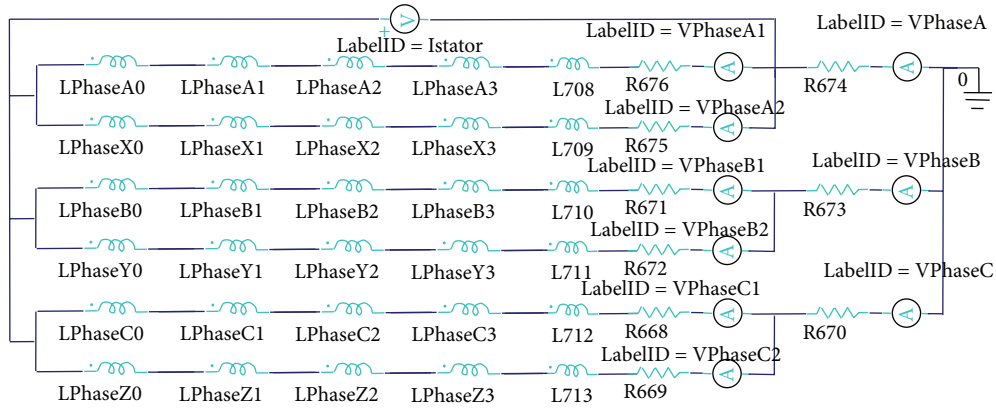

(d) External coupling circuit for the stator winding

FIGURE 7: Simulation model of SDF-9 type generator.

3.2. Results and Discussions

3.2.1. Influence on Axial UMP. The axial UMPs due to different AAGEs are indicated in Figure 10. It is easy to see that the axial UMPs will be increased as AAGE is enlarged, while in normal condition the axial UMP is about zero. The minus values of the UMPs indicate that the direction of the UMP is opposite to that of AAGE. These results are in accordance with the previous analysis.

To indicate the UMPs more clearly, a comparison between the theoretical result and the simulating result is taken, as shown in Figure 11.

Theoretically, the axial UMP in normal condition (without AAGE) should be zero. However, the simulating result shows that there is a very tiny UMP existing (see Figure 11(a)), this is mainly caused by the round-off error of the computer.

As indicated in Figure 11(a), the simulating result is generally in accordance with the theoretical ones. Meanwhile, the proposed RMS method has a closer result to the simulation data. In the cases of 2 mm, 4 mm, 6 mm, 8 mm, and 10 mm AAGEs, the relative errors for the conformal transformation method (based on (4)) are 23.2833%, 19.1762%, 14.4429%, 13.9130%, and 12.1637%, respectively, while the relative errors for the conducting paper model method are 0.8559%, 9.6911%, 18.2000%, 22.1290%, and 26.9630%, respectively. However, the relative errors for the proposed RMS method are 13.6431%, 7.6813%, 0.8772%, 1.1315%, and 4.5557%, respectively, which are much smaller than the other two methods.

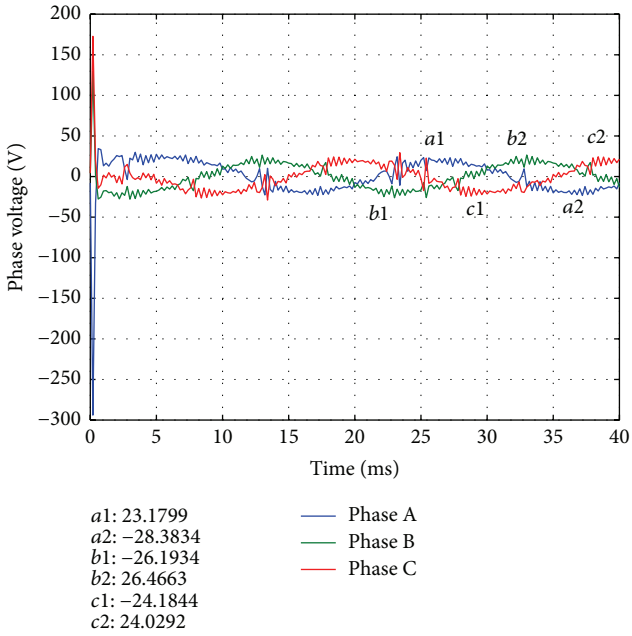

Figure 8: Phase voltage waves under normal condition.

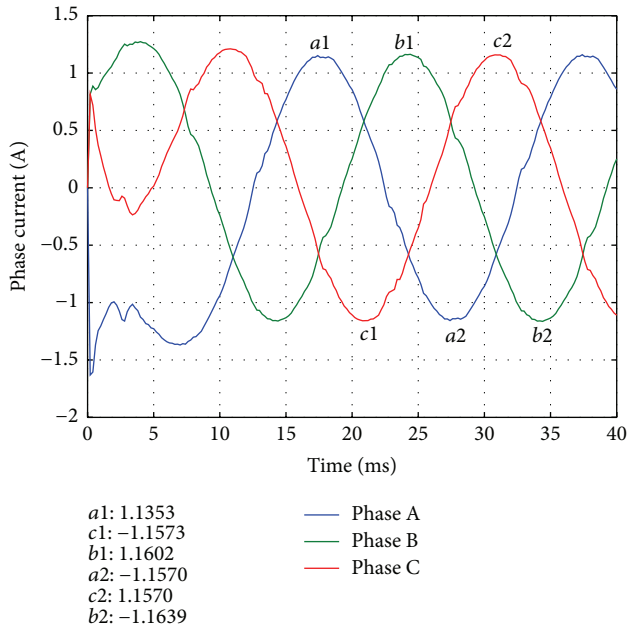

Figure 9: Phase current waves under normal condition.

Since the SDF-9 type generator is not able to carry out the experiment of AAGE faults, we take another 1600-kW generator, which has been studied and tested in [6], for a data verification, as indicated in Figure 11(b). It is shown that the simulating result and the RMS method result obtained by our work are consistent with the experimental data. This means that the FEM simulation result is viable to be treated as a verification reference and the proposed RMS method is effective. Since the proposed RMS method has a much closer result to

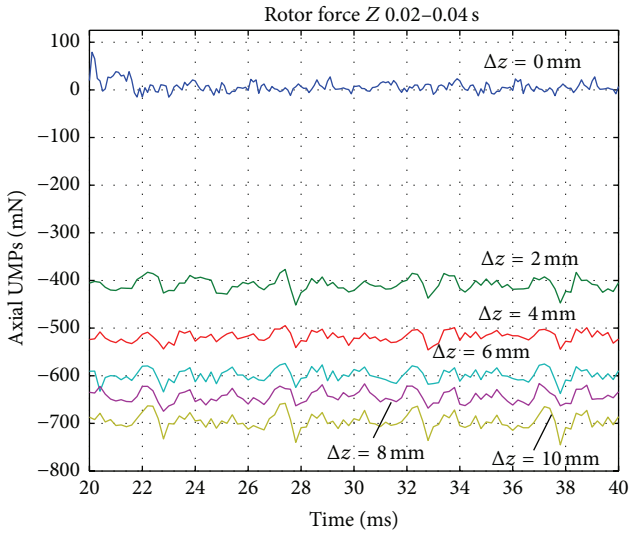

Figure 10: Axial UMP waves under different eccentricity conditions.

Table 5: Absolute average values of EMT due to different AAGEs.

AAGE (Δz/mm)	Torque (T_e/mN·m)
2	91.1881
4	88.7512
6	85.6524
9	83.5094
10	82.2145

the simulation data for the SDF-9 type generator, objectively, this method is reasonable to be thought as more accurate than the conformal transformation method and the conducting paper model method.

3.2.2. Influence on EMT. EMT results due to different AAGEs are indicated in Figures 12 and 13 and Table 5.

EMT curves in Figure 12 are retrieved from a stable period of time (0.02 s–0.04 s). In Figure 13, a clearer result can be seen by zooming in the particular sections in Figure 12. The absolute average values of the four curves in Figure 12 are calculated, as shown in Table 5.

Figure 13 and Table 5 indicate that as AAGE is increased, the absolute average values of EMT will be decreased. According to (8), the EMT T_e is proportional to the effective axial length of the rotor and stator l. Thus, as AAGE is increased, l will be decreased, resulting in the fact that EMT T_e is decreased. The simulation result qualitatively proves that EMT is inversely proportional to AAGE.

3.2.3. Influence on Stator Phase Current. The stator currents of Phase A due to different AAGEs are indicated in Figures 14–16.

The phase current curves in Figure 14 are retrieved from a stable period of time (0.02 s–0.04 s). In Figures 15 and 16,

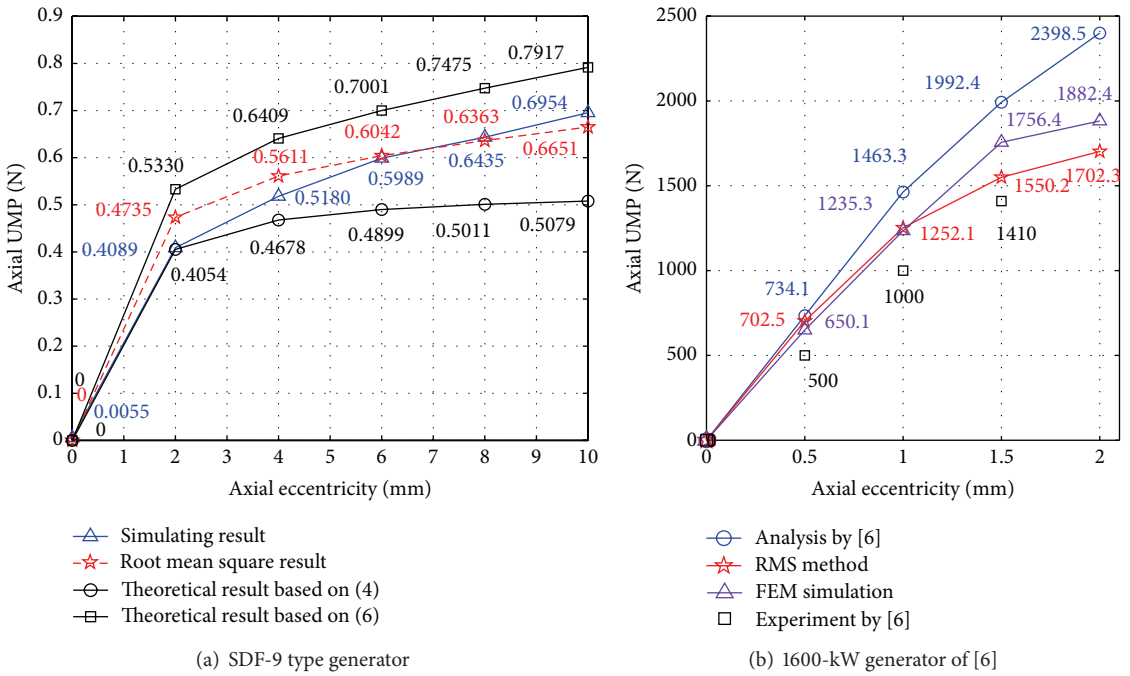

(a) SDF-9 type generator

(b) 1600-kW generator of [6]

Figure 11: Comparison between theoretical and simulating result.

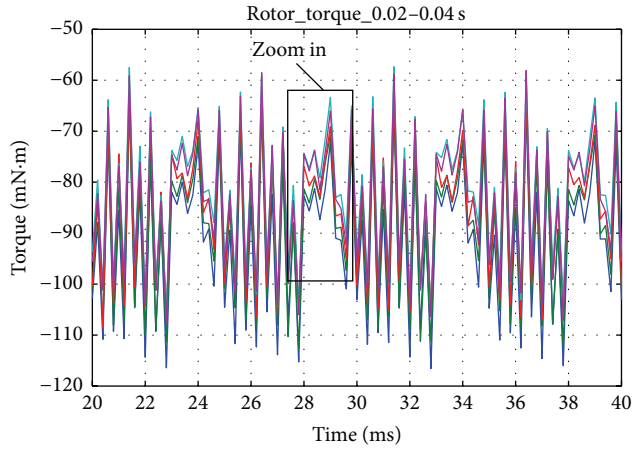

Figure 12: Relationship between axial displacement and the electromagnetic torque.

clearer results can be seen by zooming in the peaks and the valleys of Figure 14.

Figures 15 and 16 show that as AAGE is increased, the peak-to-peak values will be decreased. On the other hand, the peak-to-peak value is proportional to the effective value of I, so it is clear that the stator phase current can be influenced by AAGE and the effective value of stator phase current is inversely proportional to AAGE.

3.2.4. Influence on MFD. MFD in normal condition is indicated in Figure 17.

To study the tendency of the MFD, cloud maps of different sections due to different AAGEs in the front and the back directions are extracted, as shown in Figure 18.

The MFD results in Figure 18 are retrieved from the same time ($t = 0.03$ s) and the same range. On the front side, the MFD of the rotor end is decreased as AAGE is increased, while the MFD of the stator end is basically unchanged. Conversely, on the back side, the MFD of the stator end is decreased as AAGE is increased, while the MFD of the rotor end is basically unchanged.

The above results prove that the axial UMP and MDP will be enlarged as AAGE is increased and the direction of AAGE is opposite to that of UMP.

4. Conclusions

(1) According to (4) and (6), axial UMP should be larger but not linear as AAGE is increased and the directions

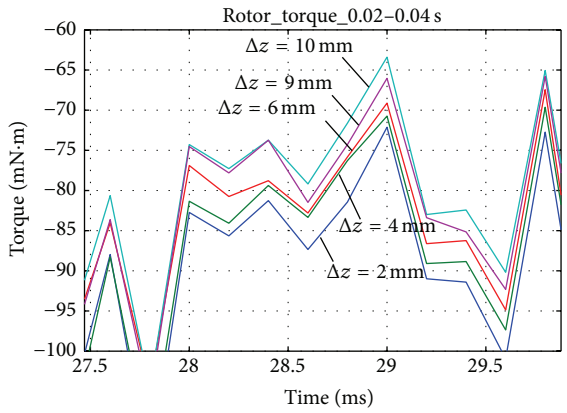

Figure 13: Enlarged view of the electromagnetic torque.

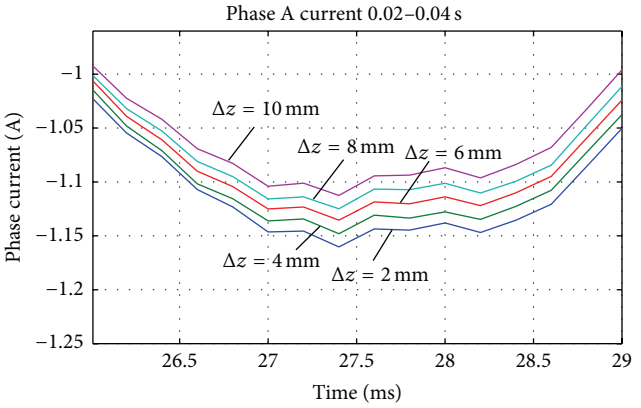

Figure 16: Enlarged view of the stator phase current (valleys).

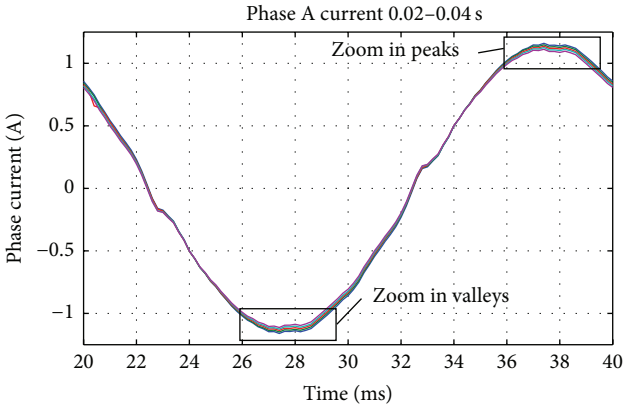

Figure 14: Relationship between axial displacement and stator phase current (Phase A).

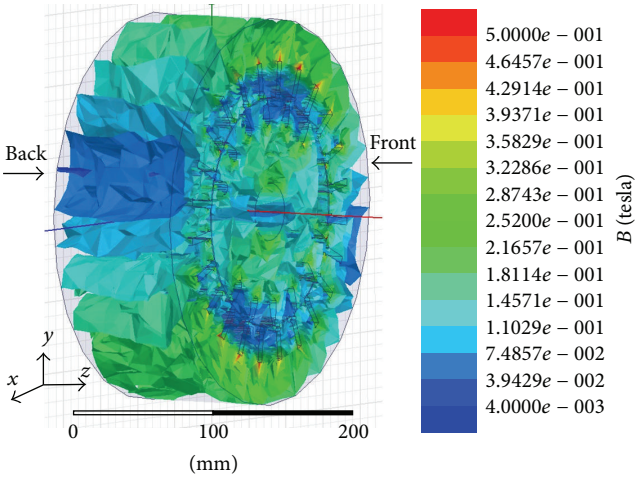

Figure 17: Magnetic density cloud map of SDF-9 type generator.

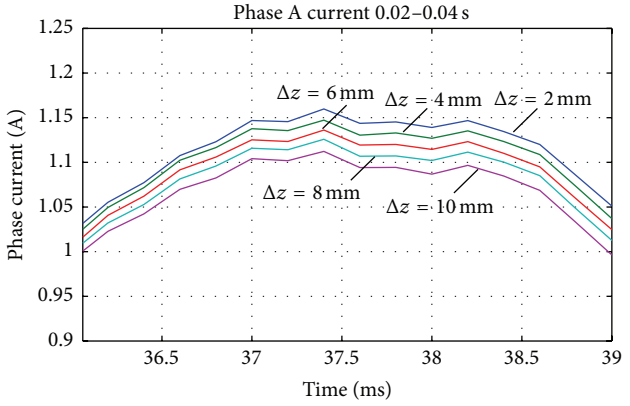

Figure 15: Enlarged view of the stator phase current (peaks).

between the axial UMP and AAGE are opposite. Moreover, a new calculation method combining (4) and (6) is proposed. The new method is to take the root mean square (RMS) value of (4) and (6). The simulation result is in accordance with the theoretical result based on (8).

(2) Qualitatively, EMT is inversely proportional to AAGEs and the simulation results are found to be in close agreement with the theories.

(3) AAGE will have an impact on the stator phase current and the phase current will be decreased as AAGE is increased.

(4) By comparing the MFD cloud maps under different AAGEs, it is shown that the MFDs on the rotor and the stator ends which are more far from the equilibrium position will be decreased as AAGE is increased, while the MFD of the stator and the rotor ends which are closer to the equilibrium position will be basically kept stable.

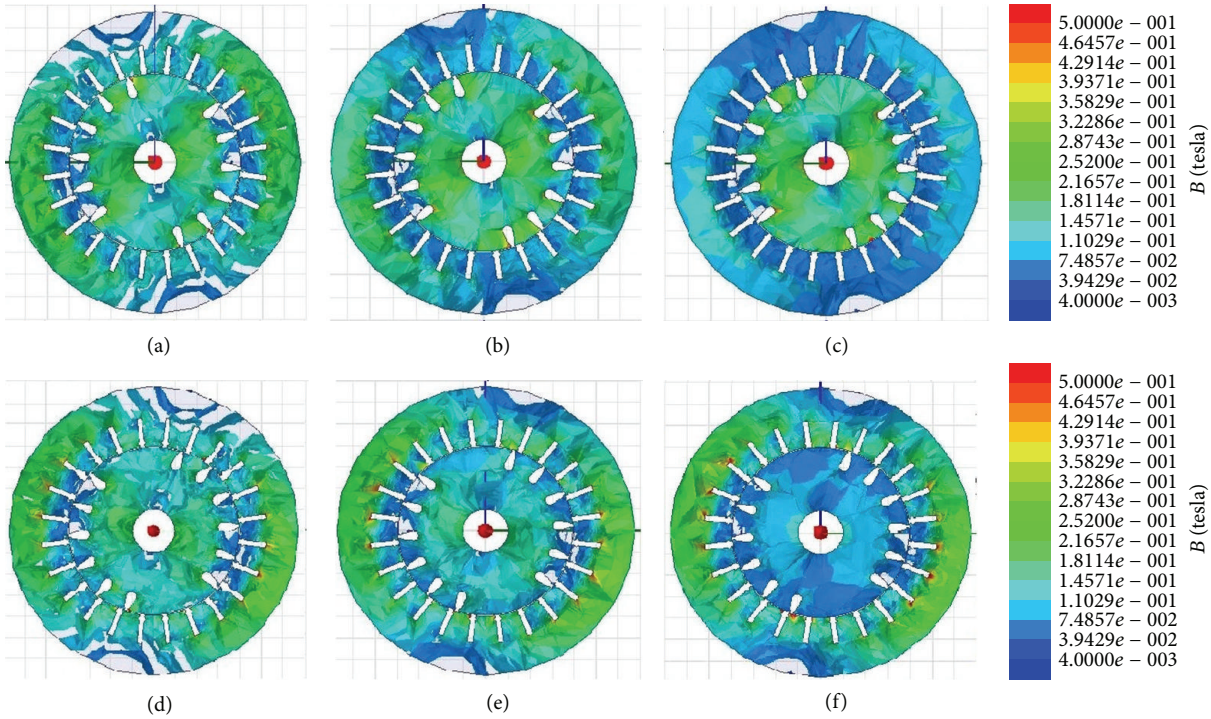

FIGURE 18: Section MFD distribution, respectively, under (a) 0 mm AAGE (back), (b) 5 mm AAGE (back), (c) 10 mm AAGE (back), (d) 0 mm AAGE (front), (e) 5 mm AAGE (front), and (f) 10 mm AAGE (front).

Conflict of Interests

The authors declare that there is no conflict of interests regarding the publication of this paper.

Acknowledgments

This work is supported by the National Natural Science Foundation of China (no. 51307058), the Natural Science Foundation of Hebei Province, China (E2014502052 and E2015502013), and the Chinese Fundamental Research Funds for the Central Universities (2015ZD27).

References

[1] Z.-Q. Song and Z.-Y. Ma, "Nonlinear vibration analysis of an eccentric rotor with unbalance magnetic pull," *Journal of Vibration and Shock*, vol. 29, no. 8, pp. 169–173, 2010.

[2] S.-T. Wan, H.-M. Li, and Y.-G. Li, "Analysis on vibration characteristics of generator with the fault of eccentric air-gap," *Journal of Vibration and Shock*, vol. 24, no. 6, pp. 21–23, 2005.

[3] L. Wang, R. W. Cheung, Z. Ma, J. Ruan, and Y. Peng, "Finite-element analysis of unbalanced magnetic pull in a large hydrogenerator under practical operations," *IEEE Transactions on Magnetics*, vol. 44, no. 6, pp. 1558–1561, 2008.

[4] Z. Jia-hui, Q. A-rui, and T. Guo, "Branch voltage of a salient pole synchronous generator with eccentric rotor and skewed slots," *Journal of Tsinghua University (Science and Technology)*, vol. 48, no. 4, pp. 453–456, 2008.

[5] S.-T. Wan, Y.-L. He, and G.-J. Tang, "Analysis on stator circulating current characteristics under eccentricity faults of turbogenerator," *High Voltage Engineering*, vol. 36, no. 6, pp. 1547–1553, 2010.

[6] K.-C. Kim, D.-H. Koo, and J. Lee, "Analysis of axial magnetic force distribution due to the axial clearance for electrical rotating machine," *IEEE Transactions on Magnetics*, vol. 43, no. 6, pp. 2546–2548, 2007.

[7] J. Y. Kim, S. J. Sung, and G. H. Jang, "Characterization and experimental verification of the axial unbalanced magnetic force in brushless DC motors," *IEEE Transactions on Magnetics*, vol. 48, no. 11, pp. 3001–3004, 2012.

[8] Y.-K. Kim, J.-J. Lee, J.-P. Hong, and Y. Hur, "Analysis of cogging torque considering tolerance of axial displacement on BLDC motor by using a stochastic simulation coupled with 3-D EMCN," *IEEE Transactions on Magnetics*, vol. 40, no. 2, pp. 1244–1247, 2004.

[9] C. E. Bradford and R. G. Rhudy, "Axial magnetic forces on induction machine rotors," *IEEE Transactions on Power Apparatus and Systems*, vol. 72, no. 2, pp. 488–494, 1953.

[10] K. Binns, "The magnetic field and centring force of displaced ventilating ducts in machine cores," *Proceedings of the IEE—Part C: Monographs*, vol. 108, no. 13, pp. 64–70, 1961.

[11] Q. D. J. Duan Wen-hui, "Axial displacement and axial electromagnetic force of rotor system in hydroturbine generator," *Journal of Mechanical Strength*, vol. 25, no. 3, pp. 285–289, 2003.

[12] P.-Z. Chen, L.-T. Yan, and R.-P. Yao, *Theory and Calculation of Electromagnetic Field*, Beijing, Science Press, Beijing, China, 1986.

[13] T. Yun-Qiu and L. Yan-ping, *Analysis and Calculation of Electromagnetic Field*, Machinery Industry Press, Beijing, China, 2010.